

Dehydration-Determined Ion Selectivity of Graphene Subnanopores

Yanjun Fu,[#] Shihao Su,[#] Ning Zhang, Yihan Wang, Xun Guo,^{*} and Jianming XueCite This: *ACS Appl. Mater. Interfaces* 2020, 12, 24281–24288

Read Online

ACCESS |

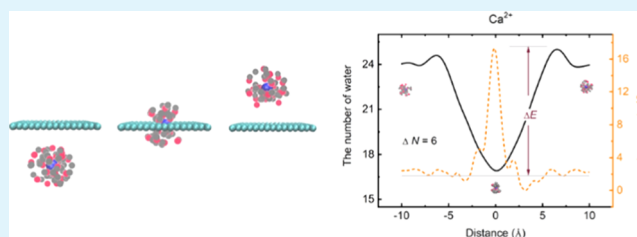
Metrics & More

Article Recommendations

Supporting Information

ABSTRACT: Graphene membranes with subnanopores are considered to be the next-generation materials for water desalination and ion separation, while their performance is mainly determined by the relative ion selectivity of the pores. However, the origin of this phenomenon has been controversial in the past few years, which strongly limits the development of related applications. Here, using direct Au ion bombardment, we fabricated the desired subnanopores with average diameters of 0.8 ± 0.16 nm in monolayer graphene. The pores showed the ability to sieve K^+ , Na^+ , Li^+ , Cs^+ , Mg^{2+} , and Ca^{2+} cations, and the observed K^+/Mg^{2+} selectivity ratio was over 4. With further molecular dynamics simulations, we demonstrated that the ion selectivity is primarily attributed to the dehydration process of ions that can be quantitatively described by the ion-dependent free-energy barriers. Hopefully, this work is helpful in further enhancing the ion selectivity of graphene nanopores and also presenting a new paradigm for improving the performance of other nanoporous atomically thin membranes, such as MXenes and MoS_2 .

KEYWORDS: ion irradiation, graphene nanopore, ion selectivity, dehydration, MD simulations



INTRODUCTION

Nowadays, due to the atomic thickness, chemical stability, and excellent mechanical properties, graphene membranes with subnanometer pores have promising potential in a wide range of applications, such as water desalination^{1–6} and matter separation.^{7–13} The related application performance of graphene subnanopores strongly depend on the ion selectivity of these subnanopores. For instance, in lithium extraction from salt-lake brines, the absolute separation efficiency is determined by the relative selectivity of lithium against other salt ions.¹⁴ Besides, the conversion efficiency in energy harvesting, i.e., converting the salinity gradient energy to electricity, also strongly relies on the ability to sieve different types of ions.^{15,16} Unfortunately, the current ion selectivity of graphene subnanopores is far from the expectation for industrial uses, due to the lack of clear understanding as to which factor is mostly influencing the ion selectivity. Hence, it is of great value to study its underlying mechanism, which has generated increasing interest in the past few years.^{17–23}

Although there are many different conjectures about the origin of ion selectivity of graphene subnanopores, this phenomenon still lacks a clear understanding and solid agreement. For example, Karnik et al.¹⁷ attributed the higher rejection of Allura Red than NaCl for graphene nanopores to the electrostatic interactions between the ions and the negative charges at the edge of the pores. With molecular dynamics (MD) simulations, Zhang et al.¹⁸ also pointed out that the charge interactions resulted in the higher rejection ratio of Mg^{2+} than K^+ . Nevertheless, Kang et al.²⁴ and Gong et al.²⁵ thought that the rejection of NaCl in forward osmosis in the

graphene membrane was primarily governed by size exclusion. Similarly, Chen et al.²⁰ showed that the high purification of Li^+ from the mixed solution with Li^+ , K^+ , Na^+ , and Cl^- ions was due to the lowest steric exclusion by calculations. Besides the two above factors, there are still some other factors that could influence the selectivity of ions. Zwolak et al.²¹ attributed the selectivity of K^+ over Cl^- to the dehydration process. Considering the intact hydration shell of ions (K^+ and Cl^-), Striolo et al.²⁶ pointed out that the diameter of pores should be exceeding ~ 7 Å for ions to pass through. Sint et al.²³ and Corry et al.²² theoretically reported that the ion transport might be related to the chemical structure of the graphene pores that could alter ion transport. In general, the experimental data on the behavior of ion transport through smaller graphene nanopores (< 2 nm) is limited,²⁷ while further related explorations, including experimental studies together with valid simulations, are urgently needed in this area.

However, it is quite challenging to explore this problem in experiments because of the difficulties in introducing qualified graphene subnanopores.^{2,11–13,28–31} Some widely used fabrication approaches, like high-temperature annealing, ozone treatment using ultraviolet (UV) light, and hydrogen plasma etching, tend to create randomly located and irregular

Received: February 29, 2020

Accepted: April 30, 2020

Published: April 30, 2020



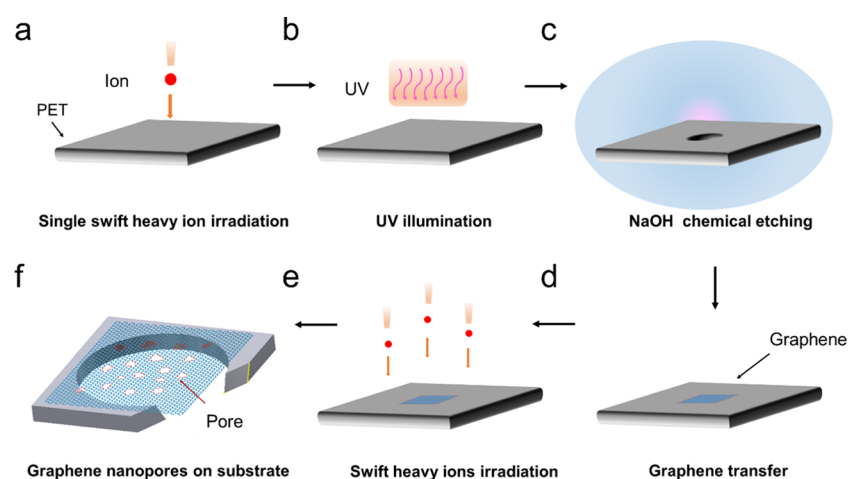


Figure 1. Schematic illustration of the fabrication of the subnanopores in the graphene membrane supported on a PET foil. (a) Single latent track inside the PET foil was employed by a swift heavy ion bombardment. (b) Each side of the irradiated PET foil was exposed to ultraviolet (UV) light for 1 h to induce photodecomposition of the damaged molecules in the latent track. (c) Single hole in the PET foil was fabricated after NaOH chemical etching. (d) Transferring the single-layer graphene on the PET support foil. (e) Graphene was perpendicularly irradiated by ions to introduce subnanopores. (f) Schematic diagram of the graphene pores on the PET foil.

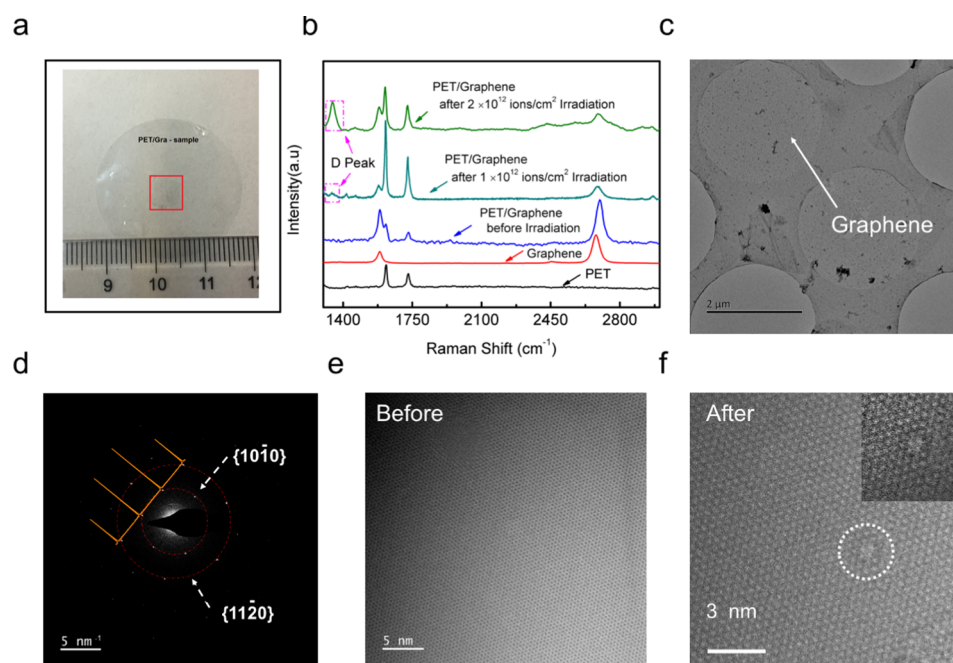


Figure 2. Characterization of the subnanopores in the graphene membrane. (a) Graphene composite membrane consisting of graphene fixed on the PET foil. (b) Raman spectrum of the PET foil, pristine graphene, the graphene composite membrane before and after irradiation with two different fluences. (c) Low-magnification image of the suspended graphene sheet on a perforated carbon foil before irradiation. (d) Selected area electron diffraction (SAED) pattern of a pristine single-layer graphene observed throughout the sample. (e–f) High-magnification topography images of the graphene membrane before and after the ion bombardment, respectively. A pore with a characteristic dimension of ~ 0.8 nm can be observed clearly.

pores.^{2,29,30} Moreover, it is hard to generate uniform nanopores smaller than 1 nm using the electrical pulse, focused electron beam, and focused ion beam techniques as well.^{11,28} Therefore, a method that can fabricate graphene subnanopores with desired diameters and numerical densities is urgently needed to investigate the ion selectivity.

In this work, using direct swift heavy ion bombardment without extra treatments, we successfully introduced nanopores with average diameters of 0.8 ± 0.16 nm and approximate density of 5×10^9 cm^{-2} in monolayer graphene, showing the great potentials of this pore fabrication technique.

The porous graphene then exhibited considerable ion selectivity among several kinds of cations (K^+ , Na^+ , Li^+ , Cs^+ , Mg^{2+} , and Ca^{2+}) in experiments. Further MD simulations were carried out to explore the main factors influencing the ion selectivity, which was also in agreement with the experiments. Combined with the MD and experimental results, we found that the ion transportation behavior in graphene subnanopores was primarily determined by the dehydration of ions, and this dehydration effect was more important than the electrostatic interaction and size exclusion for the ion selectivity of graphene pores in such a subnanometer scale.

RESULTS AND DISCUSSION

A 12 μm thick polyethylene terephthalate (PET) foil with a single embedded hole of 1.5 μm^2 in area was used as the graphene support material, whose fabrication process is schematically illustrated in Figure 1a–c. The details of the procedure are provided in the Methods, and Figure S2 shows the scanning electron microscopy image of PET holes formed in the same conditions as an example. After the introduction of the hole, a single-layer graphene was transferred onto the PET foil, as shown in Figure 1d (see Figure 2a for the photograph of the graphene/PET composite membrane used in experiments). Then, we used Au ion bombardment with energy of 500 keV and fluence of 2×10^{12} ions/ cm^2 to introduce pores in the graphene membrane (Figure 1e,f). According to our previous studies, irradiation of heavy ions with low energy can directly produce subnanometer pores in monolayer graphene^{32–34} without extra pre- or post-treatments, such as subsequent chemical oxidation.³¹ This direct irradiation method could avoid some disadvantages of other fabrication techniques, such as enlarging the intrinsic defects in graphene^{2,30} and generating irregular pores,^{17,35} which would result in active crystal boundaries.^{12,31}

Aberration-corrected transmission electron microscopy (AC-TEM, Titan Themis) was employed to obtain the atomic morphology of the graphene membrane, where the microscope was operated at 80 kV to avoid additional electron damage to the sample as the same with previous studies.^{2,17,31} Figure 2c shows the low-magnification image of graphene before irradiation, and its selected area electron diffraction (SAED) pattern is presented in Figure 2d. The SAED pattern was a typically hexagonal result, labeled with Miller–Bravais ($hkil$) indices, and the intensity of $\{110\}$ spots was obviously higher than that of $\{1120\}$ spots, which indicated that our graphene membrane was indeed a monolayer. Figure 2e shows the high-magnification image of the sample with few intrinsic defects, which agreed with the Raman spectrum results that no detectable D peak (reflecting the degree of damage) of the graphene was found (see Figure 2b). After the fabrication of nanopores, we found that the average diameters of the pores were 0.80 ± 0.16 nm, and one of them is presented in Figure 2f as an example (see the Supporting Information for more pore images and statistical analyses), where the corresponding inserted photograph shows the detail of the pore edge structure after Hanning Window image filtering processes. We further used an analytical model of the pore conductance¹¹ to obtain the density of the formed pores, and it was estimated to be 5×10^9 cm^{-2} (the transmembrane conductance for the porous graphene measured in 1 M standard KCl electrolyte solution was close to 23 nS).

In addition, Raman spectra were used to confirm the presence of the pores in graphene (see the Supporting Information for more analyses of the Raman results), and the results are shown in Figure 2b, where a clear D-band defect peak at ~ 1350 cm^{-1} in the spectrum was indeed observed (green lines), compared to pristine graphene (blue line). It is worth noting that the number of observed graphene pores in AC-TEM was limited and not enough to provide a valid pore size distribution because of the low pore density and containments like organic residuals on the membrane. Up to now, graphene subnanopores with exactly expected densities and pore diameters were successfully fabricated using direct ion bombardment (avoiding the enlargement of the intrinsic

defects and generating irregular pores in graphene because of secondary chemical etching), in which the interaction effect of ion transport from adjacent pores is far enough to be neglected,²⁷ thus favoring subsequent research studies.

The nanoporous graphene was then used to study the ion selectivity, including monovalent cations (K^+ , Na^+ , Li^+ , Cs^+), divalent cations (Mg^{2+} and Ca^{2+}), and anions (Cl^-). It should be noted that there was no valid current signal to be detected before ion irradiation (~ 0.01 nA), indicating the excellent coverage of the graphene membrane supported on PET foil. First, we studied K^+ and Cl^- , as they had similar bulk mobility.¹¹ With the Goldman–Hodgkin–Katz (GHK) model (see the Supporting Information for details), we found that the measured reversal potential V_{rev} was 294.6 mV, as shown in Figure 3b. In consideration of the redox potentials at the

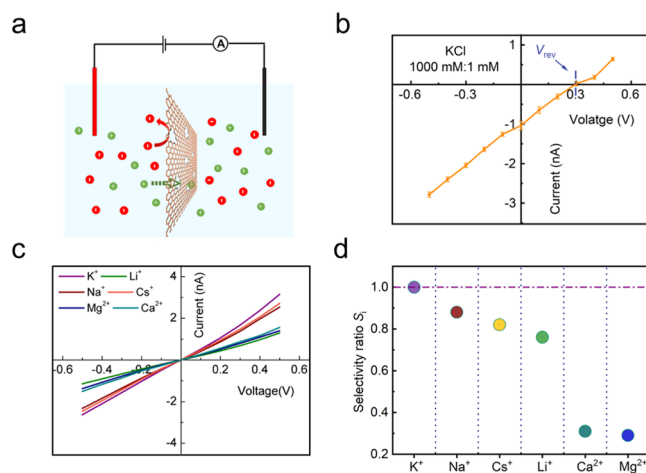


Figure 3. Relative ion selectivity of the graphene subnanopores. (a) Schematic experimental setup. (b) Representative I – V curve for the graphene pore in KCl solution with a concentration gradient of 1000. (c) Voltage–current characteristics of several kinds of cations transporting through the graphene pores. All of the concentrations of the cation-chloride solutions were maintained at 100 mM. (d) Selectivity ratio S_i of the graphene pores among different cations.

electrodes, we found that the corresponding selectivity ratio for K^+ over Cl^- is about 219. That is, most anions were impeded, as shown in Figure 3a; therefore, their contribution to ion conductance could be neglected, which has also been demonstrated in previous studies.^{11,15,36} Hence, only the transport of cations was considered in our work, which provided essential conditions to study cation selectivities of the pores, as shown below.

Afterward, we studied the ion selectivity for different cations that reflected the difficulty for ions to pass through the pores.^{11,37} Figure 3c shows the ion current through the graphene pores in different cation-chloride solutions (KCl, NaCl, LiCl, CsCl, MgCl_2 and CaCl_2) measured in experiments at a series of low voltages, where the concentrations of all of the electrolytes were maintained at 100 mM. According to Rollings et al.'s work,¹¹ the inter-cation selectivity ratio S_i (relative to K^+) was defined as $S_i = g_i/g_K$, where g_i was the normalized conductance for each type of cations (e.g., g_K for K^+). The larger the S_i was, the more easily the cation i transported through the pore compared to K^+ , and $S_i = S_j$ indicated that the cations i and j were of the same transport capability. The normalized conductance g_i satisfied $g_i = G_i/(\mu_i Q_i/\mu_{\text{K}^+})$, where G_i was the measured conductance through

the graphene pores for different cations i , μ_i was the bulk electrophoretic mobility of the cation i , and Q_i was the transferred electric charges of the cation i . The reason for introducing g_i was that different cations had significantly different electrophoretic mobilities in bulk solutions (listed in Table 1), as well as diverse transferred electric charges, which would influence the measured pore conductance.

Table 1. Electrophoretic Mobility, Hydration Energy, and Hydrated Ion Radius for K^+ , Na^+ , Li^+ , Cs^+ , Mg^{2+} , and Ca^{2+} ^a

cation	electrophoretic mobility μ_i 10^{-4} ($cm\ s^{-1})/(V\ cm^{-1})$	relative mobility μ_i/μ_{K^+}	hydration energy (kcal/mol)	hydrated ion radii (Å)	Ref.
K^+	7.62	1.00	70	3.31	38
Na^+	5.19	0.68	87	3.58	38
Li^+	4.01	0.53	113	3.82	38
Cs^+	8.01	1.05	97	3.29	39
Ca^{2+}	6.17	0.81	357	4.12	38
Mg^{2+}	5.50	0.72	434	4.28	38

^aThe relative mobility of other cations to K^+ is also presented to quantify the relative variation of mobility among all of these cations.

As shown in Figure 3d, the S_i of all cations measured in experiments was in the order of $S_K > S_{Na} > S_{Cs} > S_{Li} \gg S_{Ca} > S_{Mg}$, which was the same as Rollings et al.'s work,¹¹ indicating that our graphene subnanopores had a capability of distinguishing these cations. The pores showed a strong discrimination ability between monovalent and divalent cations, e.g., S_K being about four times higher than S_{Mg} , indicated that the K^+ was much easier to pass through the pores than Mg^{2+} . According to Figure 3d and Table 1, S_i decreased with the increasing ion hydration energy and hydrated radius. As a result, we speculated that the ion hydration properties might be one of the key factors influencing the ion relative selectivity, and further investigated it in the following sections.

To study the ion transport through graphene subnanopores in atomic scale and explore the primary factor of selectivity, MD simulations were employed here, by constructing a monolayer graphene with a single pore, whose size was consistent with our observation in experiments (about 0.85 nm in diameter), and the charge density at the pore edge was $-0.2\ C/m^2$ in accordance with the previous experimental results.⁴⁰ It is worth noting that the origin of the negative charges is not well understood yet, and the reasons may be the deprotonation of the edge groups^{17,31} or surface contamination;⁴¹ therefore, we equivalently set the negative charges on the pore edge as the same with other works.^{15,36} The Lennard-Jones (LJ) potential was used to describe the ion interaction, whose parameters (ϵ and σ) of different cations are provided in Table 2. In the simulations, we investigated all of the cations K^+ , Na^+ ,

Table 2. LJ Potential Parameters for K^+ , Na^+ , Li^+ , Mg^{2+} , Ca^{2+} , and C–O Bond Used in MD Simulations

cations	q (e)	ϵ (kcal/mol)	σ (Å)	Ref.
K^+	+1	0.1247	3.250	36
Na^+	+1	0.3526	2.160	42
Li^+	+1	0.1039	1.440	43
Mg^{2+}	+2	0.9153	1.398	44
Ca^{2+}	+2	0.4704	2.361	44
C–O		0.1143	3.275	36

Li^+ , Mg^{2+} , and Ca^{2+} , except for Cs^+ , because there were no reliable LJ parameters for Cs^+ in graphene. The simulation setup is schematically illustrated in Figure 4a, where the graphene sheet is fixed in the middle of the box and the electrolyte solution concentration is set to be 1 mol/L.

The ion fluxes through the simulated graphene subnanopore were first studied, which had the sequence of $K^+ > Na^+ > Li^+ > Ca^{2+} > Mg^{2+}$ at different electric field intensities E (see Figure 4b). We found that the relative order of the simulated ion fluxes of different cations was consistent with the experimental results, as shown in Figure 4c, further proving the validity of our MD simulations. In addition, there was a significant linear correlation ($R^2 = 0.91$) between them as well, indicating that the simulated ion fluxes could qualitatively fit the experimental results to some extent. The normalized ion fluxes of all cations (by K^+) are presented in Figure 4e (note that the difference of ions' electrophoretic mobility was not considered in the calculation of the normalized ion flux), and the order was also consistent with our experimental results as shown in Figure 3d. Considering that there was indeed an obvious correlation between the experimental and simulated ion flux, we believed that MD simulations could also represent the discrimination ability of the graphene pore, even though the difference of ions' electrophoretic mobility was not eliminated in the analysis of simulation results.

As mentioned before, the ion dehydration might be the primary factor influencing the relative ion selectivity. Therefore, we investigated the hydration status of Na^+ and Ca^{2+} cations as examples when they were transporting through the constructed pore, i.e., staying in different simulation windows along the potential of mean force (PMF) profiles. The radial distribution function (RDF) $g(r)$ at different locations of ions and oxygen atoms in water molecules (ions– O_w) was calculated, which reflected the hydration structure and shell of the ions. Figure 5a,b indicates that there were two distinct peaks in the RDF of Ca^{2+} (Ca^{2+} – O_w), whereas only one in that of Na^+ (Na^+ – O_w). The results confirmed that the hydrated Ca^{2+} had two water shells and Na^+ had one water shell.^{44,45} Besides, we found that the hydration radii of Na^+ and Ca^{2+} were 3.06 and 4.34 Å respectively, which also agreed with the results in previous works.^{44,45}

Then, we studied the spatial evolution of water molecules inside the hydration shells of Na^+ and Ca^{2+} cations when they were passing through the graphene pore by taking the integral of $g(r)$. As shown in Figure 5c,d, the number of hydrated water molecules was first decreased (close to the pore) and then increased (away from the pore) for both Na^+ and Ca^{2+} , and the maximum drop of the water molecules ΔN was about 2 for Na^+ and 6 for Ca^{2+} , respectively. In addition, the PMF profiles of the cations were further calculated, as shown in Figure 5c,d with the right vertical axes. Obviously, there was a negative correlation between the ions' energy (comparing its thermodynamic free diffusion state) and the number of its surrounding water molecules. According to Zwolak et al.'s work,²¹ the ion-dependent free-energy barrier was indeed mainly contributed from the ion's dehydration process. For Na^{2+} , as an example shown in Figure 5c, the closer it approached the pore center, the less surrounding water molecules it had, and the higher the energy was. Therefore, ion-dependent free-energy barrier ΔE could reflect the difficulty of dehydration of ions to pass through the pore. We found that the energy barrier of Ca^{2+} was larger than that of Na^+ (due to its stronger electrostatic interaction with water

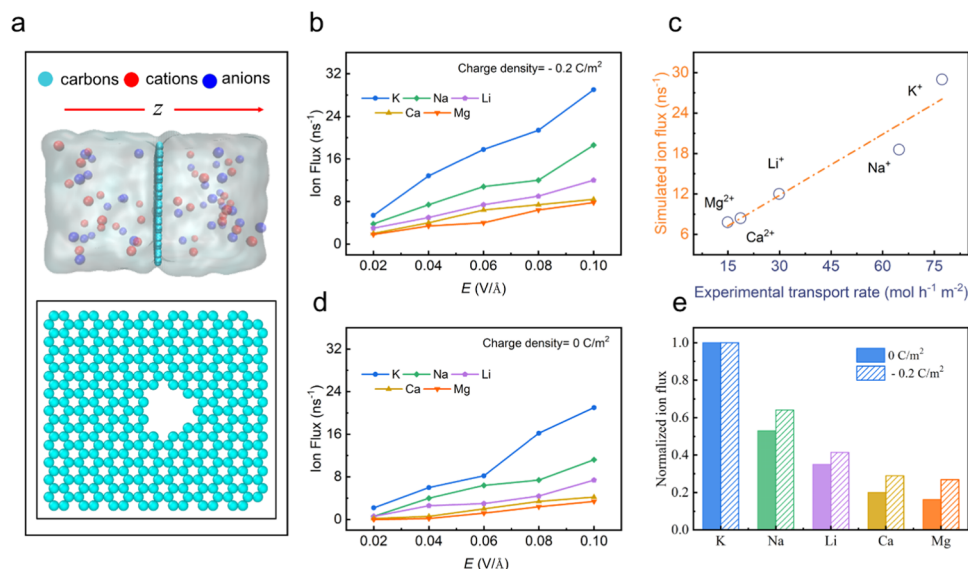


Figure 4. Study of relative ion selectivity of graphene subnanopores. (a) Schematic illustration of the MD simulation system. (b) Ion fluxes of different cations through the negatively charged pore as a function of the electric field intensity E . (c) Simulated ion flux ($E = 0.1 \text{ V/\AA}$) vs the experimental transport rate for various cations (blue circles). The dashed line is a linear fit ($R^2 = 0.91$) to the data. (d) Ion fluxes of different cations through the uncharged pore as a function of E . (e) Normalized ion fluxes of all cations (by K^+) through the pore at 0.1 V/\AA in simulations.

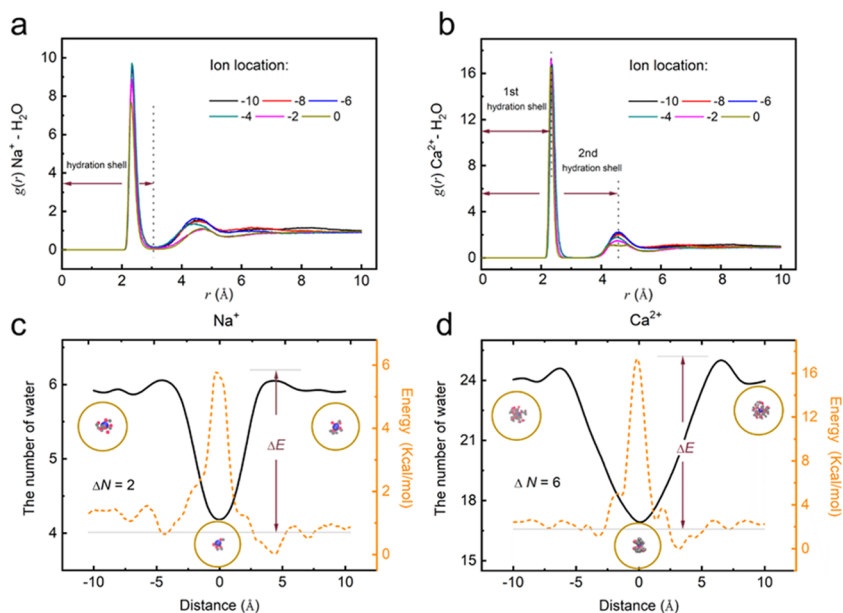


Figure 5. Dehydration of Na^+ and Ca^{2+} when transporting through the negatively charged graphene pore. (a) Ion–water RDF for Na^+ and water. (b) Ion–water RDF for Ca^{2+} and water. The horizontal axis r meant the distance between the water molecules and the ion, and the legend is the location of the ion in different simulation windows along PMF profiles (as schematically shown in Figure 4a). The number of water molecules surrounding (c) Na^+ and (d) Ca^{2+} against the distance between the ion and the pore center along the z -axis (displayed in Figure 4a) when the ion is located in different positions. The insets schematically illustrate the hydration status of the ion, where the brown circle represents its hydration shell structure, and the hydrogen and oxygen atoms in water molecules are displayed as lime and magenta balls, respectively. The right-hand axis is the energy of the ion, which is compared with the energy of its thermodynamic free diffusion state (lower gray line). The marked difference of ΔE is the so-called ion-dependent free-energy barrier.

molecules); therefore, the flux of Ca^{2+} should be lower than that of Na^+ , which has already been proved by our experimental and simulation results (see Figures 3c and 4b). Briefly, the dehydration process of ions, yielding ion-dependent free-energy barriers, primarily determined the relative ion selectivity for graphene subnanopores. Figure 6 shows the energy barriers for all of the cations (K^+ , Na^+ , Li^+ , Mg^{2+} , and Ca^{2+}), whose order was $\text{K}^+ < \text{Na}^+ < \text{Li}^+ < \text{Ca}^{2+} < \text{Mg}^{2+}$,

indicating that K^+ was the easiest to dehydrate when passing through the pore. As a result, K^+ should naturally be of the highest ion flux and inter-cation selectivity ratio, as shown in Figures 3d and 4e.

We also studied the influence of the electrostatic interaction and size exclusion, two other main factors mentioned before in the manuscript, on the ion selectivity of graphene subnanopores. First, we made the pore uncharged and calculated

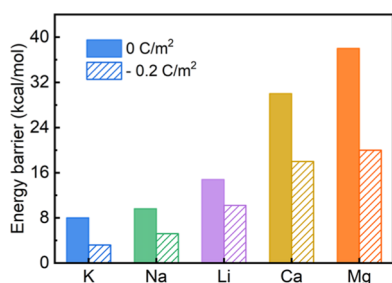


Figure 6. Ion-dependent free-energy barrier for cations to pass through the pore along the z -axis (the direction is as schematically shown in Figure 4a).

the ΔE of all cations, whose results are shown in Figure 6. When the pore was not charged, ΔE of every kind of cation was much larger than that for the negatively charged one, because the electrostatic interaction between the cations and negative charges at the pore edge could facilitate the dehydration of cations and decrease ΔE . Therefore, the fluxes of all of the cations through the uncharged pore were decreased, as shown in Figure 4d.

Figure 4e indicates that the uncharged graphene subnanopore would still have the ability to sieve different cations. To confirm this, we conducted some special experiments where the pH of the electrolyte was set to 2.76 to make the previous negatively charged graphene subnanopores turn into neutral ones according to previous work,⁴⁰ and the results together with the corresponding calculations are presented in the Supporting Information. In these experiments, different ions (e.g., K^+ and Cl^-) indeed exhibited considerably different relative selectivities in the neutral subnanopores, as shown in Table S2. When the pores were not charged, the electrostatic interaction between the pore edge and the ions could be neglected. Thus, the different ion selectivities observed in both experiments and simulations (as shown in Figure S3) could be primarily ascribed to the ion dehydration instead of the electrostatic interaction as reported before.^{11,17,31}

We then investigated the influence of the size exclusion mechanism by constructing a new larger graphene pore with a diameter of 1.2 nm (close to the diameter of the largest graphene pore occasionally found by us in experiments, see the Supporting Information) and negatively charged with -0.2 C/m² as well. The simulated result of the 1.2 nm diameter pore is shown in Figure S4, which showed that the pore still had the discrimination capability among cations. As the pore size was obviously larger than all of the cations' diameters listed in Table 1, the size exclusion had slight influences on the ion selectivity, indicating that the dehydration process (due to the reorientation of the hydration shell somehow) is still a dominant cause.

CONCLUSIONS

We fabricated graphene subnanopores by direct ion irradiation and then studied the transport behaviors of different ions through the pores in experiments. With further MD simulations, the dehydration of ions was found to mainly dominate the ion selectivity of the pores, and the difficulty of the ion dehydration could be reflected by the ion-dependent free-energy barrier. According to the results, monovalent cations can pass more easily through the graphene subnanopores than the divalent cations because the former dehydrate water molecules more easily (due to their smaller

energy barriers as shown in Figure 6), indicating that the pores are more effective in discriminating these two kinds of cations. Our work of the dehydration-determined ion selectivity of graphene subnanopores may further lead to a wide range of potential applications like hydrated ion sensors, nanofiltration membranes for aquo-complex separation, and voltage-tunable nanofluidic devices.

METHODS

PET Foil Substrate Fabrication. Our experiments were conducted on ion-track-etched single nanopore embedded in the polyethylene terephthalate (PET) membrane, which was initially irradiated with a single swift heavy ion (Ar) with energy of 6.17 MeV/u. Then, the processed foil was mounted in a custom-designed system in a 60 °C thermal bath and chemically etched with a 2 M NaOH etchant. The fabrication of a single hole in the PET membrane is shown in Figure 1a–c, which could also be seen in our previous work.^{13,40} The diameter of the PET hole could be estimated via the following equation: $D = \sqrt{4LI/\pi\kappa U}$, where L is the foil thickness, and I , U , and κ are the measured current, applied voltage, and electrolyte conductivity, respectively.⁴¹ By plugging in the experimental data, the diameter of the fabricated hole was found to be 1.4 μ m.

Transfer of Graphene to PET Foil. The single-layer graphene membrane, grown by chemical vapor deposition on a copper foil, was transferred onto a perforated PET foil using the standard wet transfer procedure,^{31,46} which is schematically illustrated in Figure 1d–f. First, polymethyl-methacrylate (PMMA, Aldrich Prod. No. 445746, dissolved in anisole with concentration of 40 mg/mL) was spin-coated (first 2000 rpm for 40 s and later 4000 rpm for 60 s) onto the top surface of the graphene. Then, the PMMA layer was cured at 80 °C in ambient conditions for 5 min, followed by the etching of the copper substrate in 0.5 M $FeCl_3$ solutions to obtain the PMMA/graphene composite membrane. Subsequently, the film was washed several times in 1 M HCl solution and deionized water to remove residual etchants. Finally, the PMMA/graphene membrane was transferred onto a prepared PET foil, and acetone steam was used to dissolve PMMA to obtain the graphene supported by the PET substrate in the end.

Fabrication and Characterization of Graphene Nanopore. The transferred graphene (supported by the PET film for studies of ion selectivity or by the TEM grid for observation) was perpendicularly irradiated by 500 keV Au ions with a fluence of 2×10^{12} ions/cm² at room temperature to create nanopores in the 2×1.7 MeV serial electrostatic accelerator at Peking University, Beijing, China. The graphene sample for TEM characterization was transferred onto a holey carbon TEM grid (with 2 μ m holes, Ted Pella, Inc.) using the procedure described in refs. 31, 47 before ion irradiation. First, the TEM grid with an amorphous-carbon side was placed on the surface of graphene (grown on a copper foil as mentioned above), and then several drops of isopropyl alcohol were gently dropped on it. After the isopropyl alcohol evaporated, the graphene attached to the TEM grid. Subsequently, the sample was heated at 140 °C for 10 min to increase the adhesion between graphene and the TEM grid. Finally, the copper substrate in the composite Cu/graphene/TEM grid membrane was etched using APS-100 (10–20% ammonium persulfate), followed by washing in 1 M HCl solutions and deionized water three times, the same as that in the transfer of graphene to PET foil.

MD Simulation. MD simulation was carried out using the large-scale atomic/molecular massively parallel simulator (LAMMPS) package⁴⁸ and visualized with visual molecular dynamics (VMD).⁴⁹ The adaptive intermolecular reactive empirical bond-order potential functions were employed to describe the interactions between the carbon atoms in the graphene.⁵⁰ Water molecules were described by the TIP3P model.⁵¹ All of the cations were described by the LJ potentials, as summarized in Table 2, where the mixing parameters for the potentials between different elements were derived from the

Lorentz–Berthelot combining rules.⁴³ Periodic boundary conditions were imposed along all three orthogonal directions. All through the calculations, a cutoff of 10.0 Å was used for the LJ potentials, and the long-range Coulomb forces were computed using the particle–particle–mesh solver. The nanopore in graphene was constructed by removing the corresponding carbon atoms with a distance to the pore center smaller than the designated radius. The simulations were carried out using a box of $34 \times 31 \times 54$ Å³. During PMF profile calculations, the reaction coordinate along the pore axial was divided into 21 windows with a width of 1 Å, and each window was run for 2 ns. After applying an electric field on the simulations, the system was initially run for 2 ns to achieve a steady velocity, while the statistical data were collected for the last 10 ns.

■ ASSOCIATED CONTENT

SI Supporting Information

The Supporting Information is available free of charge at <https://pubs.acs.org/doi/10.1021/acsami.0c03932>.

Images of created graphene subnanopores and statistical analyses; Raman analyses of graphene membrane; Goldman–Hodgkin–Katz model; K⁺/Cl[−] selectivity with respect to the pH value; SEM image of holes on the PET substrate; transport properties of a 0.8 nm uncharged graphene pore and transport properties of a 1.2 nm negatively charged graphene pore (PDF)

■ AUTHOR INFORMATION

Corresponding Author

Xun Guo – State Key Laboratory of Nuclear Physics and Technology, School of Physics, Peking University, Beijing 100871, P. R. China; orcid.org/0000-0002-8424-2618; Email: guo.xun@pku.edu.cn

Authors

Yanjun Fu – State Key Laboratory of Nuclear Physics and Technology, School of Physics and CAPT, HEDPS, College of Engineering, Peking University, Beijing 100871, P. R. China; orcid.org/0000-0003-0308-8098

Shihao Su – State Key Laboratory of Nuclear Physics and Technology, School of Physics and CAPT, HEDPS, College of Engineering, Peking University, Beijing 100871, P. R. China; orcid.org/0000-0001-7568-2155

Ning Zhang – State Key Laboratory of Nuclear Physics and Technology, School of Physics and CAPT, HEDPS, College of Engineering, Peking University, Beijing 100871, P. R. China

Yihan Wang – State Key Laboratory of Nuclear Physics and Technology, School of Physics and CAPT, HEDPS, College of Engineering, Peking University, Beijing 100871, P. R. China

Jianming Xue – State Key Laboratory of Nuclear Physics and Technology, School of Physics and CAPT, HEDPS, College of Engineering, Peking University, Beijing 100871, P. R. China

Complete contact information is available at: <https://pubs.acs.org/doi/10.1021/acsami.0c03932>

Author Contributions

[#]Y.F. and S.S. contributed equally to this work.

Author Contributions

X.G. and J.X. conceived the research. Y.F. and S.S. performed the experiment and data analysis. Y.F. and X.G. performed the MD simulations. X.G., J.X., Y.F., S.S., N.Z. and Y.W. prepared the manuscript. All authors discussed the results, commented on the manuscript, and contributed to the writing of the paper.

Notes

The authors declare no competing financial interest.

■ ACKNOWLEDGMENTS

This work was funded by the National Natural Science Foundation of China (NSFC, Grant Nos. 11705010 and 11775005), the China Postdoctoral Science Foundation (Grant No. 2019M650351), the Science Challenge Project (No. TZ2018004), and funding support from the State Key Laboratory of Nuclear Physics and Technology, Peking University (No. NPT2019ZZ01). We are grateful for computing resource provided by Weiming No. 1 and Life Science No. 1 High-Performance Computing Platform at Peking University, and TianHe-1(A) at the National Super-computer Center in Tianjin.

■ REFERENCES

- (1) Han, Y.; Xu, Z.; Gao, C. Ultrathin Graphene Nanofiltration Membrane for Water Purification. *Science* **2013**, *23*, 3693–3700.
- (2) Surwade, S. P.; Smirnov, S. N.; Vlassiuk, I. V.; Unocic, R. R.; Veith, G. M.; Dai, S.; Mahurin, S. M. Water Desalination Using Nanoporous Single-Layer Graphene. *Nat. Nanotechnol.* **2015**, *10*, 459–464.
- (3) Werber, J. R.; Osuji, C. O.; Elimelech, M. Materials for Next-Generation Desalination and Water Purification Membranes. *Nat. Rev. Mater.* **2016**, *1*, No. 16018.
- (4) Xie, M.; Shon, H. K.; Gray, S. R.; Elimelech, M. Membrane-Based Processes for Wastewater Nutrient Recovery: Technology, Challenges, and Future Direction. *Water Res.* **2016**, *89*, 210–221.
- (5) Choi, K.; Droudian, A.; Wyss, R. M.; Schlichting, K.-P.; Park, H. G. Multifunctional Wafer-Scale Graphene Membranes for Fast Ultrafiltration and High Permeation Gas Separation. *Sci. Adv.* **2018**, *4*, No. eaau0476.
- (6) Mi, B. Scaling up Nanoporous Graphene Membranes. *Science* **2019**, *364*, 1033–1035.
- (7) Abraham, J.; Vasu, K. S.; Williams, C. D.; Gopinadhan, K.; Su, Y.; Cherian, C. T.; Dix, J.; Prestat, E.; Haigh, S. J.; Grigorieva, I. V.; Carbone, P.; Geim, A. K.; Nair, R. R. Tunable Sieving of Ions Using Graphene Oxide Membranes. *Nat. Nanotechnol.* **2017**, *12*, 546–550.
- (8) Yang, Y.; Yang, X.; Liang, L.; Gao, Y.; Cheng, H.; Li, X.; Zou, M.; Ma, R.; Yuan, Q.; Duan, X. Large-Area Graphene-Nanomesh/Carbon-Nanotube Hybrid Membranes for Ionic and Molecular Nanofiltration. *Science* **2019**, *364*, 1057–1062.
- (9) Esfandiari, A.; Radha, B.; Wang, F. C.; Yang, Q.; Hu, S.; Garaj, S.; Nair, R. R.; Geim, A. K.; Gopinadhan, K. Size Effect in Ion Transport through Angstrom-Scale Slits. *Science* **2017**, *358*, 511–513.
- (10) Celebi, K.; Buchheim, J.; Wyss, R. M.; Droudian, A.; Gasser, P.; Shorubalko, I.; Kye, J.-I.; Lee, C.; Park, H. G. Ultimate Permeation Across Atomically Thin Porous Graphene. *Science* **2014**, *344*, 289–292.
- (11) Rollings, R. C.; Kuan, A. T.; Golovchenko, J. A. Ion Selectivity of Graphene Nanopores. *Nat. Commun.* **2016**, *7*, No. 11408.
- (12) Zhao, J.; He, G.; Huang, S.; Villalobos, L. F.; Dakhchoune, M.; Bassas, H.; Agrawal, K. V. Etching Gas-Sieving Nanopores in Single-Layer Graphene with an Angstrom Precision for High-Performance Gas Mixture Separation. *Sci. Adv.* **2019**, *5*, No. eaav1851.
- (13) He, G.; Huang, S.; Villalobos, L. F.; Zhao, J.; Mensi, M.; Oveisi, E.; Rezaei, M.; Agrawal, K. V. High-Permeance Polymer-Functionalized Single-Layer Graphene Membranes that Surpass the Post-combustion Carbon Capture Target. *Energy Environ. Sci.* **2019**, *12*, 3305–3312.
- (14) Zhao, Y.; Shi, W.; Van der Bruggen, B.; Gao, C.; Shen, J. Tunable Nanoscale Interlayer of Graphene with Symmetrical Polyelectrolyte Multilayer Architecture for Lithium Extraction. *Adv. Mater. Interfaces* **2018**, *5*, No. 1701449.

- (15) Fu, Y.; Guo, X.; Wang, Y.; Wang, X.; Xue, J. An Atomically-Thin Graphene Reverse Electrodialysis System for Efficient Energy Harvesting from Salinity Gradient. *Nano Energy* **2019**, *57*, 783–790.
- (16) Feng, J.; Graf, M.; Liu, K.; Ovchinnikov, D.; Dumcenco, D.; Heiranian, M.; Nandigana, V.; Aluru, N. R.; Kis, A.; Radenovic, A. Single-Layer MoS₂ Nanopores as Nanopower Generators. *Nature* **2016**, *536*, 197–200.
- (17) O'Hern, S. C.; Jang, D.; Bose, S.; Idrobo, J.-C.; Song, Y.; Laoui, T.; Kong, J.; Karnik, R. Nanofiltration across Defect-Sealed Nanoporous Monolayer Graphene. *Nano Lett.* **2015**, *15*, 3254–3260.
- (18) Yan, Y. G.; Wang, W. S.; Li, W.; Loh, K. P.; Zhang, J. A Graphene-Like Membrane with an Ultrahigh Water Flux for Desalination. *Nanoscale* **2017**, *9*, 18951–18958.
- (19) Joshi, R. K.; Carbone, P.; Wang, F. C.; Kravets, V. G.; Su, Y.; Grigorieva, I. V.; Wu, H. A.; Geim, A. K.; Nair, R. R. Precise and Ultrafast Molecular Sieving through Graphene Oxide Membranes. *Science* **2014**, *343*, 752–754.
- (20) Li, K.; Tao, Y.; Li, Z.; Sha, J.; Chen, Y. Selective Ion-Permeation through Strained and Charged Graphene Membranes. *Nanotechnology* **2017**, *29*, No. 035402.
- (21) Sahu, S.; Di Ventra, M.; Zwolak, M. Dehydration as a Universal Mechanism for Ion Selectivity in Graphene and Other Atomically Thin Pores. *Nano Lett.* **2017**, *17*, 4719–4724.
- (22) He, Z.; Zhou, J.; Lu, X.; Corry, B. Bioinspired Graphene Nanopores with Voltage-Tunable Ion Selectivity for Na⁺ and K⁺. *ACS Nano* **2013**, *7*, 10148–10157.
- (23) Sint, K.; Wang, B.; Král, P. Selective Ion Passage through Functionalized Graphene Nanopores. *J. Am. Chem. Soc.* **2008**, *130*, 16448–16449.
- (24) Gai, J.-G.; Gong, X.-L.; Wang, W.-W.; Zhang, X.; Kang, W.-L. An Ultrafast Water Transport Forward Osmosis Membrane: Porous Graphene. *J. Mater. Chem. A* **2014**, *2*, 4023–4028.
- (25) Gai, J.-G.; Gong, X.-L. Zero Internal Concentration Polarization FO Membrane: Functionalized Graphene. *J. Mater. Chem. A* **2014**, *2*, 425–429.
- (26) Konatham, D.; Yu, J.; Ho, T. A.; Striolo, A. Simulation Insights for Graphene-Based Water Desalination Membranes. *Langmuir* **2013**, *29*, 11884–11897.
- (27) Wang, L.; Boutilier, M. S. H.; Kidambi, P. R.; Jang, D.; Hadjiconstantinou, N. G.; Karnik, R. Fundamental Transport Mechanisms, Fabrication and Potential Applications of Nanoporous Atomically Thin Membranes. *Nat. Nanotechnol.* **2017**, *12*, 509–522.
- (28) Buchheim, J.; Wyss, R. M.; Shorubalko, I.; Park, H. G. Understanding the Interaction between Energetic Ions and Free-standing Graphene towards Practical 2D Perforation. *Nanoscale* **2016**, *8*, 8345–8354.
- (29) Liu, L.; Ryu, S.; Tomasik, M. R.; Stolyarova, E.; Jung, N.; Hybertsen, M. S.; Steigerwald, M. L.; Brus, L. E.; Flynn, G. W. Graphene Oxidation: Thickness-Dependent Etching and Strong Chemical Doping. *Nano Lett.* **2008**, *8*, 1965–1970.
- (30) Wu, S.; Yang, R.; Shi, D.; Zhang, G. Identification of Structural Defects in Graphitic Materials by Gas-Phase Anisotropic Etching. *Nanoscale* **2012**, *4*, 2005–2009.
- (31) O'Hern, S. C.; Boutilier, M. S. H.; Idrobo, J.-C.; Song, Y.; Kong, J.; Laoui, T.; Atieh, M.; Karnik, R. Selective Ionic Transport through Tunable Subnanometer Pores in Single-Layer Graphene Membranes. *Nano Lett.* **2014**, *14*, 1234–1241.
- (32) Li, W.; Liang, L.; Zhao, S.; Zhang, S.; Xue, J. Fabrication of Nanopores in a Graphene Sheet with Heavy Ions: A Molecular Dynamics Study. *J. Appl. Phys.* **2013**, *114*, No. 234304.
- (33) Zhao, S.; Xue, J.; Liang, L.; Wang, Y.; Yan, S. Drilling Nanopores in Graphene with Clusters: A Molecular Dynamics Study. *J. Phys. Chem. C* **2012**, *116*, 11776–11782.
- (34) Guo, X.; Fu, Y.; Zhang, X.; Wang, X.; Chen, Y.; Xue, J. A Semi-Classical Model for the Charge Exchange and Energy Loss of Slow Highly Charged Ions in Ultrathin Materials. *Matter Radiat. Extremes* **2019**, *4*, No. 054401.
- (35) Goyal, G.; Lee, Y. B.; Darvish, A.; Ahn, C. W.; Kim, M. J. Hydrophilic and Size-controlled Graphene Nanopores for Protein Detection. *Nanotechnology* **2016**, *27*, No. 495301.
- (36) Zhao, S.; Xue, J.; Kang, W. Ion Selection of Charge-Modified Large Nanopores in a Graphene Sheet. *J. Chem. Phys.* **2013**, *139*, No. 114702.
- (37) Park, H. B.; Kamcev, J.; Robeson, L. M.; Elimelech, M.; Freeman, B. D. Maximizing the Right Stuff: The Trade-Off between Membrane Permeability and Selectivity. *Science* **2017**, *356*, No. eaab0530.
- (38) Nightingale, E. R., Jr. Phenomenological Theory of Ion Solvation. Effective Radii of Hydrated Ions. *J. Phys. Chem. A* **1959**, *63*, 1381–1387.
- (39) Ali, S. M.; De, S.; Maity, D. K. Microhydration of Cs⁺ Ion: A Density Functional Theory Study on Cs⁺-(H₂O)_n Clusters (n = 1–10). *J. Chem. Phys.* **2007**, *127*, No. 044303.
- (40) Shan, Y. P.; Tiwari, P. B.; Krishnakumar, P.; Vlassiuk, I.; Li, W. Z.; Wang, X. W.; Darici, Y.; Lindsay, S. M.; Wang, H. D.; Smirnov, S.; He, J. Surface Modification of Graphene Nanopores for Protein Translocation. *Nanotechnology* **2013**, *24*, No. 495102.
- (41) Konkena, B.; Vasudevan, S. Understanding Aqueous Dispersibility of Graphene Oxide and Reduced Graphene Oxide through pKa Measurements. *J. Phys. Chem. Lett.* **2012**, *3*, 867–872.
- (42) Joung, I. S.; Cheatham, T. E. Determination of Alkali and Halide Monovalent Ion Parameters for Use in Explicitly Solvated Biomolecular Simulations. *J. Phys. Chem. B* **2008**, *112*, 9020–9041.
- (43) Aragones, J. L.; Rovere, M.; Vega, C.; Gallo, P. Computer Simulation Study of the Structure of LiCl Aqueous Solutions: Test of Non-Standard Mixing Rules in the Ion Interaction. *J. Phys. Chem. B* **2014**, *118*, 7680–7691.
- (44) Chen, B.; Jiang, H.; Liu, X.; Hu, X. Molecular Insight into Water Desalination across Multilayer Graphene Oxide Membranes. *ACS Appl. Mater. Interfaces* **2017**, *9*, 22826–22836.
- (45) Chen, B.; Jiang, H.; Liu, X.; Hu, X. Observation and Analysis of Water Transport through Graphene Oxide Interlamination. *J. Phys. Chem. C* **2017**, *121*, 1321–1328.
- (46) Goniszewski, S.; Gallop, J. C.; Adabi, M.; Gajewski, K.; Shaforost, E.; Klein, N.; Sierakowski, A.; Chen, J.; Chen, Y.; Gotszalk, T.; Hao, L. Self-Supporting Graphene Films and Their Applications. *IET Circuits Devices Syst.* **2015**, *9*, 420–427.
- (47) Regan, W.; Alem, N.; Alemán, B.; Geng, B.; Girit, Ç.; Maserati, L.; Wang, F.; Crommie, M.; Zettl, A. A Direct Transfer of Layer-Area Graphene. *Appl. Phys. Lett.* **2010**, *96*, No. 113102.
- (48) Plimpton, S. Fast Parallel Algorithms for Short-Range Molecular Dynamics. *J. Comput. Phys.* **1995**, *117*, 1–19.
- (49) Humphrey, W.; Dalke, A.; Schulten, K. VMD: Visual Molecular Dynamics. *J. Mol. Graphics* **1996**, *14*, 33–38.
- (50) Brenner, D. W.; Shenderova, O. A.; Harrison, J. A.; Stuart, S. J.; Ni, B.; Sinnott, S. B. A Second-Generation Reactive Empirical Bond Order (REBO) Potential Energy Expression for Hydrocarbons. *J. Phys.: Condens. Matter* **2002**, *14*, 783–802.
- (51) Jorgensen, W. L.; Chandrasekhar, J.; Madura, J. D. Comparison of Simple Potential Functions for Simulating Liquid Water. *J. Chem. Phys.* **1983**, *79*, 926–935.